dinates. The extremely short lifetime of the excited state (~50 fs), as established by transient absorption (*17*), resonance Raman intensity analysis (*25*), and spontaneous fluorescence measurements (*26*), however, severely restricts the extent of atomic displacements that can occur on this time scale. Given the energy available to the chromophore, the maximum C_{11}=C_{12} dihedral angle that can be achieved in 50 fs is ~50°, even if restrictions from the protein pocket are ignored (*25*, *27*). This suggests that the role of C_{11}=C_{12} torsional motion during the excited-state lifetime is limited. The similarity of the vibrational period of the 969 cm^{-1} $C_{11}H$=$C_{12}H$ HOOP (~36 fs) to the excited-state lifetime (~50 fs) supports its role in facilitating internal conversion. Additionally, resonance Raman intensity analysis shows quantitatively that retinal undergoes rapid distortion along the $C_{11}H$=$C_{12}H$ HOOP coordinate after optical excitation as a consequence of the lowered overall symmetry of the molecule when bound to rhodopsin (*25*). We thus conclude that excited-state decay through a conical intersection is mediated largely by fast HOOP motion.

Evolution along the C_{11}=C_{12} torsional coordinate after internal conversion leads to the formation of photorhodopsin with a formally isomerized (>90°) C_{11}=C_{12} bond but an overall highly distorted structure. Adjacent single- and double-bond twists compensate for the local cis-trans isomerization resulting in an overall reactant-like shape that, although isomerized about the C_{11}=C_{12} bond, minimizes steric interactions with the protein pocket, thereby enabling the fast reaction rate (compare Fig. 3, A and B). The molecule then uses the ~5000 cm^{-1} of energy available from rapid barrierless internal conversion as well as the ~3000 cm^{-1} from the photo-to-batho relaxation to drive the larger scale structural changes necessary to form the all-trans bathorhodopsin photoproduct in ~1 ps (Fig. 3C). Thus, although the isomerization is initiated in the excited state and photorhodopsin is formally trans about the C_{11}=C_{12} bond, much of the geometric changes associated with the isomerization actually occur on the ground potential surface in the photo-to-batho transition. This result is a direct consequence of the different time scales for complete excited-state decay (~200 fs) and bathorhodopsin formation (~1 ps) determined in this work.

This multidimensional model for rhodopsin isomerization, including a fast "gating" coordinate (HOOP), deviates substantially from the one-dimensional picture commonly used to describe photoisomerization reactions, where both electronic and nuclear dynamics occur along the same, slow torsional coordinate. Furthermore, these observations make it possible to better understand the role of the protein in determining rhodopsin's unique reactivity. The tight binding pocket influences the reaction path in three ways: (i) It primes the molecule for rapid excited-state decay along the HOOP coordinate by pretwisting the retinal backbone, (ii) it restricts the possible motion of the excited chromophore through steric interactions with surrounding amino acids, thereby promoting reaction speed and resulting in a high isomerization quantum yield, and (iii) it captures the high-energy bathorhodopsin product and efficiently transfers this energy into protein conformational changes that activate the receptor. We anticipate that these concepts will be important in understanding many efficient photobiological reactions.

References and Notes

1. C. V. Shank, *Science* **233**, 1276 (1986).
2. A. H. Zewail, *Femtochemistry* (World Scientific, Singapore, 1994).
3. G. R. Fleming, R. van Grondelle, *Curr. Opin. Struct. Biol.* **7**, 738 (1997).
4. M. M. Martin, J. T. Hynes, Eds., *Femtochemistry and Femtobiology: Ultrafast Events in Molecular Science* (Elsevier, Amsterdam, 2004).
5. L. Zhu, J. T. Sage, P. M. Champion, *Science* **266**, 629 (1994).
6. F. Schotte *et al.*, *Science* **300**, 1944 (2003).
7. M. D. Fayer, Ed., *Ultrafast Infrared and Raman Spectroscopy* (Marcel Dekker, New York, 2001).
8. H. Hamaguchi, T. L. Gustafson, *Annu. Rev. Phys. Chem.* **45**, 593 (1994).
9. M. C. Asplund, M. T. Zanni, R. M. Hochstrasser, *Proc. Natl. Acad. Sci. U.S.A.* **97**, 8219 (2000).
10. C. J. Fecko, J. D. Eaves, J. J. Loparo, A. Tokmakoff, P. L. Geissler, *Science* **301**, 1698 (2003).
11. S. E. Bromberg *et al.*, *Science* **278**, 260 (1997).
12. D. W. McCamant, P. Kukura, R. A. Mathies, *J. Phys. Chem. A* **107**, 8208 (2003).
13. S. Y. Lee, D. H. Zhang, D. W. McCamant, P. Kukura, R. A. Mathies, *J. Chem. Phys.* **121**, 3632 (2004).
14. Y. Mizutani, T. Kitagawa, *Science* **278**, 443 (1997).
15. The uncertainty principle is not violated because the broadband probe pulse in FSRS is dispersed and its multichannel detection is not time-resolved. In practice, the available information is only limited by the instrumental time resolution and our ability to model the experimental data.
16. W. T. Pollard, S. Y. Lee, R. A. Mathies, *J. Chem. Phys.* **92**, 4012 (1990).
17. R. W. Schoenlein, L. A. Peteanu, R. A. Mathies, C. V. Shank, *Science* **254**, 412 (1991).
18. A. Warshel, *Nature* **260**, 679 (1976).
19. R. S. H. Liu, *Acc. Chem. Res.* **34**, 555 (2001).
20. T. Andruniow, N. Ferre, M. Olivucci, *Proc. Natl. Acad. Sci. U.S.A.* **101**, 17908 (2004).
21. Materials and methods are available as supporting material on *Science* Online.
22. R. A. Mathies, J. Lugtenburg, in *Handbook of Biological Physics, Volume 3: Molecular Mechanisms in Visual Transduction*, D. G. Stavenga, W. J. DeGrip, E. N. Pugh Jr., Eds. (Elsevier, New York, 2000), pp. 55–90.
23. E. C. Y. Yan *et al.*, *Biochemistry* **43**, 10867 (2004).
24. M. J. Frisch *et al.*, Gaussian 03, Gaussian Inc., Pittsburgh, PA (2001).
25. G. R. Loppnow, R. A. Mathies, *Biophys. J.* **54**, 35 (1988).
26. G. G. Kochendoerfer, R. A. Mathies, *J. Phys. Chem.* **100**, 14526 (1996).
27. F. Blomgren, S. Larsson, *Chem. Phys. Lett.* **376**, 704 (2003).
28. K. Palczewski *et al.*, *Science* **289**, 739 (2000).

29. We thank S.-Y. Lee for many helpful discussions and S. Naghibzadeh for expert rhodopsin preparation. This work was supported in part by NIH grant EY-02051.

Supporting Online Material

www.sciencemag.org/cgi/content/full/310/5750/1006/DC1
Materials and Methods
Figs. S1 to S3
Table S1

3 August 2005; accepted 27 September 2005
10.1126/science.1118379

The Mid-Pleistocene Transition in the Tropical Pacific

Martín Medina-Elizalde[1,2] and David W. Lea[1,3]*

A sea surface temperature (SST) record based on planktonic foraminiferal magnesium/calcium ratios from a site in the western equatorial Pacific warm pool reveals that glacial-interglacial oscillations in SST shifted from a period of 41,000 to 100,000 years at the mid-Pleistocene transition, 950,000 years before the present. SST changes at both periodicities were synchronous with eastern Pacific cold-tongue SSTs but preceded changes in continental ice volume. The timing and nature of tropical Pacific SST changes over the mid-Pleistocene transition implicate a shift in the periodicity of radiative forcing by atmospheric carbon dioxide as the cause of the switch in climate periodicities at this time.

In the mid-Pleistocene, ~950 thousand years (ky) before the present (B.P.), the climate of Earth underwent profound changes in the length and intensity of its glacial cycles. This mid-Pleistocene transition (MPT), as indicated by benthic foraminiferal $\delta^{18}O$, was characterized by a change in the dominant periodicity of high-latitude climate oscillations from 41 ky to 100 ky; a positive shift in mean benthic $\delta^{18}O$, generally ascribed to continental ice-sheet expansion; and an increase in the amplitude variability of $\delta^{18}O$, attributed to more severe glaciations after 950 ky B.P. (*1*–*3*). Most of the hypotheses offered to explain these changes involve high-latitude Northern Hemisphere processes such as ice-sheet or sea-ice dynamics (*2*, *4*, *5*). Recent paleoclimatic reconstructions, however, have shown that during the MPT, the tropics also experienced major changes that resemble some aspects of high-latitude climate variability but also have their own unique patterns (*6*, *7*). Current hypotheses cannot fully explain these observations and the common

[1]Department of Earth Science, [2]Interdepartmental Program in Marine Science, [3]Marine Science Institute, University of California Santa Barbara, Santa Barbara, CA 93106–9630, USA.

*To whom correspondence should be addressed: E-mail: lea@geol.ucsb.edu

characteristics revealed by paleoclimatic reconstructions from low and high latitudes.

To test hypothesized causes for the mid-Pleistocene transition, we reconstructed detailed thermal and $\delta^{18}O$-seawater histories spanning the MPT from a site in the heart of the western equatorial Pacific (WEP) warm pool (Fig. 1). This location is ideal for testing hypotheses that address proposed forcing mechanisms of tropical climate variability because (i) warm-pool thermal variability is linked throughout the tropics by convection (*8*); (ii) the warm pool is less subject to regional oceanographic influences such as thermocline depth changes, as demonstrated by the small response of warm-pool sea surface temperatures to El Niño/Southern Oscillation (ENSO) variations (Fig. 1) (*9*); and (iii) the warm pool is remote from the direct radiative influence of continental ice sheets and has the most direct response to radiative forcing as a result of changes in atmospheric greenhouse gases (*10*, *11*).

We determined sea surface temperatures (SSTs), $\delta^{18}O$, and $\delta^{18}O$-seawater ($\delta^{18}O_w$) from Ocean Drilling Program (ODP) Hole 806B (0°19.1′N, 159°21.7′E, 2520-m water depth) (*12*) on the Ontong Java Plateau, using the surface-dwelling planktonic foraminifer *Globigerinoides ruber* (Fig. 2). Our records reach back to 1.3 million years (My) B.P., with an average resolution of 2.3 ky, extending a previous study (*13*). We used the Mg-paleothermometry technique, which is based on the temperature dependence of Mg substitution in calcite, and calculated $\delta^{18}O_w$ following previous protocols (*13*, *14*). We constructed the Hole 806B age model by visual alignment of the *G. ruber* $\delta^{18}O$ sequence to the ODP Hole 677 benthic $\delta^{18}O$ record (*14*, *15*). Hole 806B has remarkably constant sedimentation rates (2.0 ± 0.3 cm/ky) from 0.45 to 1.3 My B.P. and, because of its location above the present-day lysocline depth, it also has good preservation of foraminifer shells. There are only two coring gaps of ~0.9 m (~50 ky) that include parts of marine isotope stage (MIS) 19 and MIS 37 (*14*).

The *G. ruber* $\delta^{18}O$ data indicate 12 glacial-interglacial (G-I) oscillations from MIS 13 to 41 between 450 and 1348 ky B.P., in agreement with reference foraminiferal $\delta^{18}O$ records (*12*, *15*) (Figs. 2 and 3). Over the past 900 ky, the G-I range of $\delta^{18}O$ is larger by about one-third than the corresponding early Pleistocene (900 to 1348 ky) range, but mean $\delta^{18}O$ remains the same [–1.60 ‰ (per mil) and –1.56 ‰, respectively]. Spectral analysis of the Hole 806B $\delta^{18}O$ data indicates that over the past 900 ky, the 100-ky period component explains more than 70% of the variance in $\delta^{18}O$, whereas during the early Pleistocene (EP) similar power is shared by ~90-ky and 41-ky–related periodicities, with a minor contribution from the 23-ky period. The presence of significant power at a ~90-ky period might be the result of a strong salinity component at site 806B during the early Pleistocene (*16*).

The observed Mg/Ca-derived SST average from the early and mid-Pleistocene time intervals combined (from 500 to 1348 ky B.P.) is 27.8°C, similar to the late Pleistocene (0 to 500 ky B.P.) SST average of 27.4°C (*13*). The G-I SST range over the mid-to-early Pleistocene is smaller than that during the late Pleistocene, 3°C versus 4.3°C, respectively. This difference is largely a consequence of warmer (~0.7°C) glacial intervals, relative to the late Pleistocene; average interglacial SSTs (~29°C) are similar throughout the record. The warmest temperatures during

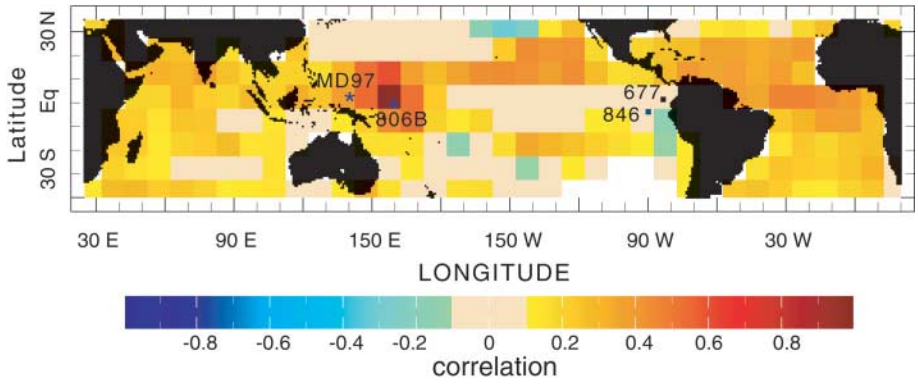

Fig. 1. Map showing the correlation of Kaplan interannual SST anomalies between the site of Hole 806B (0°19.1′N, 159°21.7′E) and other regions of the tropics (*28*). Correlations are based on SST data on a 5 by 5 grid of monthly anomalies from 1856 to 2003. The base period used for the anomalies is 1951 to 1980. Locations of ODP Hole 846 (*6*) (3°5′S, 90°49′W) and MD97-2140 (*7*) (2°02′N, 141°46′E) are also indicated. Warm-pool SST anomalies near Hole 806B are positively correlated with temperature anomalies in a wide swath of the tropical oceans. Warm-pool anomalies are either uncorrelated or are anticorrelated with anomalies in the eastern equatorial Pacific cold tongue (i.e., Hole 846), a consequence of their opposite behavior during ENSO changes (*20*). The location of ODP Hole 677 [reference benthic foraminiferal $\delta^{18}O$ record in (*15*)] is also shown (1°12′N, 83°44′W).

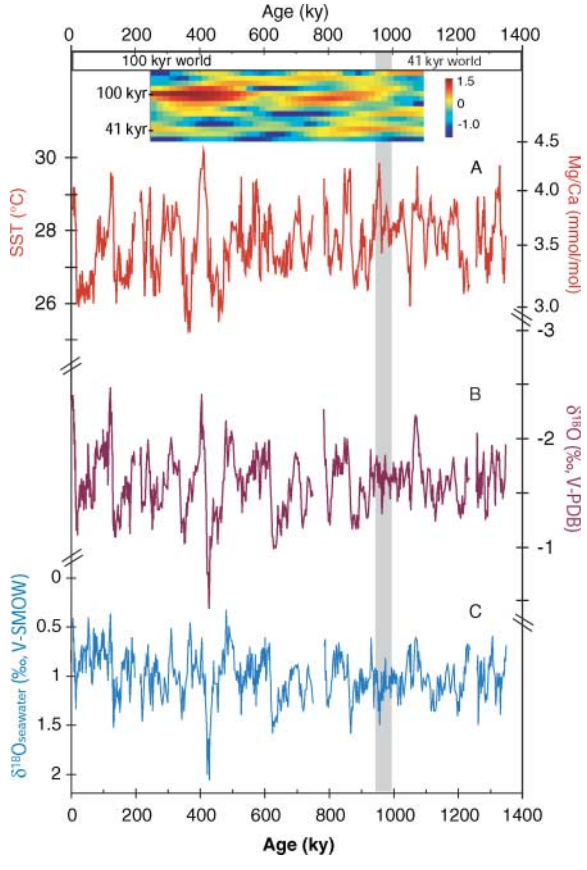

Fig. 2. Western equatorial Pacific ODP Hole 806B records based on the surface-dwelling foraminifera *G. ruber*. This record includes a previous (*13*) reconstruction for the late Pleistocene (4 to 470 ky B.P.). Gaps in the records are the result of coring gaps. The chronology is based on wiggle matching to the target core ODP Hole 677 benthic foraminiferal $\delta^{18}O$ (*14*, *15*). (**A**) *G. ruber* Mg/Ca-derived SST record. Mg/Ca data were converted using the relationship: SST (C°) = 0.089^{-1}*ln[Mg/Ca (m) / 0.3] (*13*). Each point is the average of two to four replicates. The mid-Pleistocene transition (MPT) at ~950 ky B.P. is indicated by a gray bar. Evolutionary spectral analysis plot for SST (top) from 250 to 1100 ky B.P. is based on the multitaper method (*14*). The scale represents Log_{10} units^2 per cycle per ky. The evolutionary spectral analysis reveals that the SST record is dominated by the ~100-ky period over the last 950 ky B.P. and by ~41-ky and ~60-ky–related periods from 1346 ky to 950 ky B.P. (**B**) *G. ruber* $\delta^{18}O$ record. The G-I range of $\delta^{18}O$ increases over the MPT. (**C**) $\delta^{18}O$-seawater record, calculated by extracting the component in planktonic $\delta^{18}O$ explained by the Mg/Ca-derived SST using the low-light paleotemperature equation determined for *Orbulina universa* (*29*). Neither the calcite nor the seawater $\delta^{18}O$ records shows a positive shift over the MPT.

the mid- and early Pleistocene occurred in MIS 25 (29.8°C), 952 ky B.P., and the coldest in MIS 30 (26°C), 1052 ky B.P. (Fig. 2). The mid-Pleistocene transition is well represented in the Hole 806B SST record (Fig. 2). Mean SST and the average G-I change in SST do not shift over the MPT, in contrast to changes observed in benthic $\delta^{18}O$ (Figs. 3 and 4). Average SSTs during the early and mid-Pleistocene (500 to 900 ky B.P.) are virtually identical, 27.9 ± 0.7°C and 27.7 ± 0.7°C (1 SD), respectively (Fig. 2).

The G-I range in $\delta^{18}O_w$, calculated from measured $\delta^{18}O$ and inferred temperatures, is ~0.7‰ over the full length of the record (Fig. 2). A previous study of the late Pleistocene record from Hole 806B (*13*) demonstrates that $\delta^{18}O_w$ at this site is strongly influenced by hydrological changes on G-I time scales. In addition to orbital frequencies, the $\delta^{18}O_w$ time series also shows quasiperiodic ~200-ky cycles during the early and mid-Pleistocene time interval. These cycles might be related to long-term hydrological evolution in this region, suggesting that $\delta^{18}O_w$ is not a simple proxy of ice volume at this site. The G-I range of Hole 806B $\delta^{18}O_w$ increases by ~0.16‰ during the MPT, from an early Pleistocene value of 0.72‰ to a mid-Pleistocene value of 0.88‰, which likely reflects increasing variability in continental ice as suggested by benthic foraminiferal records (*1*–*3*).

The Hole 806B SST record is spectrally similar to the ODP Hole 677 reference benthic foraminiferal $\delta^{18}O$ record (*15*), with a characteristic dominance of ~100-ky and 41-ky periods and a much weaker contribution at 23 ky (Figs. 2 and 3). As suggested by evolutionary spectral analysis of Hole 806B SST and Hole 677 benthic foraminiferal $\delta^{18}O$, the transition between the 41-ky and 100-ky–dominant modes of variability occurred at ~950 ky B.P. (Fig. 4, right panels). Point-to-point comparison between these two records over the MPT reveals that *G. ruber* SST leads benthic $\delta^{18}O$ by ~3 ky (Fig. 4). Furthermore, cross-spectral analysis between *G. ruber* SST and benthic foraminiferal $\delta^{18}O$ reveals that SST leads benthic $\delta^{18}O$ by 3 ± 1.2 ky [95% confidence interval (CI)] at the 41-ky–dominant period during the early Pleistocene.

SST records from two other sites in the tropical Pacific, one in the eastern equatorial cold tongue (*6*) and a second in the area of strong intertropical convergence zone influence northwest of our site (*7*), provide basinwide context for our records (Fig. 1). Comparison of these SST records from 1348 to 900 ky B.P. suggests a strengthening of the zonal equatorial Pacific SST gradient by ~1.3°C, due almost entirely to the cooling in the eastern Pacific. The development of this SST gradient occurred during a time interval in which there was no secular change in WEP SSTs, as revealed by the two western Pacific SST records (*7*) (Fig. 3). High-latitude climate, as indicated by the Hole 677 $\delta^{18}O$ record, was also relatively stable at this time (Fig. 3). Statistical analysis of benthic foraminiferal records and the Hole 806B $\delta^{18}O_w$ series reveal that high-latitude climate was relatively stable for more than 400 ky before the MPT (Fig. 3) (*17*). This observation suggests that the intensification of tropical Pacific zonal temperature gradients and the inferred enhancement of the Walker circulation at this time was not accompanied by regional long-term hydrological changes in the WEP and Northern Hemisphere high-latitude climate reorganizations, in contrast to previous suggestions (*7*, *18*).

The long-term surface cooling of the eastern-boundary upwelling regions from 1350 to 900 ky

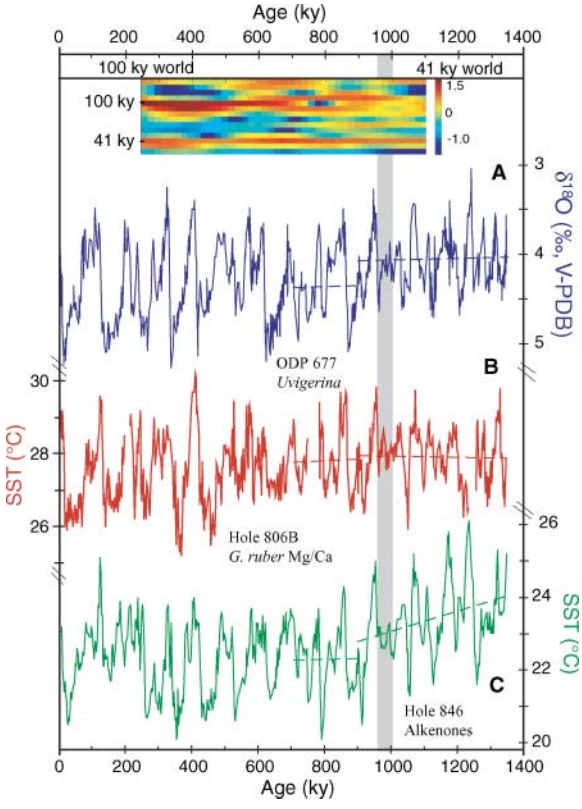

Fig. 3. (**A**) ODP Hole 677 benthic foraminiferal $\delta^{18}O$ record (*15*) showing a mean positive shift of 0.25‰ at ~900 ky B.P. and long-term stability from 1340 to 900 ky B.P. (dashed lines are linear regressions). The linear regression of $\delta^{18}O$ over this time interval is not statistically significant (*17*). Top: Spectrogram of benthic $\delta^{18}O$ from 250 to 1100 ky B.P. showing the shift in the dominant period from 100 ky to 41 ky at ~950 ky B.P. (gray bar) (*14*). The scale represents Log_{10} units^2 per cycle per ky. (**B**) Hole 806B *G. ruber* SST record showing no significant secular change from 1340 to 800 ky B.P. and long-term thermal stability over the MPT (red line before the transition represents a nonsignificant linear regression; slope = zero, 95% CI). (**C**) SST record from eastern equatorial Pacific ODP Hole 846 (3°5′S, 90°49′W) based on the alkenone unsaturation index (*6*). The statistically significant linear regression (slope ≠ zero, 95% CI) showing a secular cooling trend from 1340 to 900 ky B.P. is indicated (green line). As a consequence, from 1340 to 900 ky the equatorial Pacific temperature zonal gradient increased by ~1.3°C.

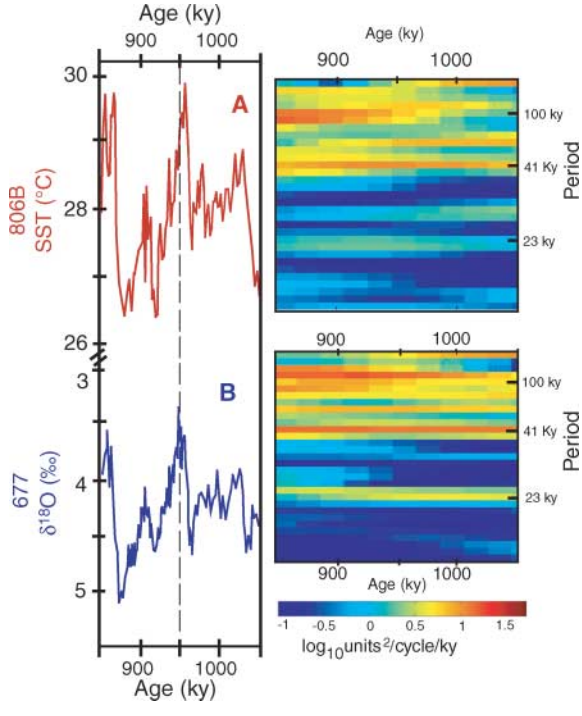

Fig. 4. Blowup of the mid-Pleistocene transition as seen in the Hole 806B SST record (**A**) and the Hole 677 benthic foraminiferal $\delta^{18}O$ record (**B**). Right panels show a blowup over the MPT of the spectrograms shown in Figs. 2 and 3. The interglacial peak centered on 950 ky B.P. is MIS 25. Note the presence of the positive shift in benthic $\delta^{18}O$ at ~900 ky B.P. and the absence of a similar shift in SST at that time. The transition between the 41-ky and 100-ky variability occurs between 950 and 1000 ky B.P. in both records. Point-to-point comparisons between the two signals suggest that SSTs lead benthic $\delta^{18}O$ by ~3 ky over the MPT. The same pattern can be seen between SST and planktonic $\delta^{18}O$ in Hole 806B (Fig. 2).

B.P. (*6*), while the warm pool and Northern Hemisphere climate remained relatively stable, may be related to secular changes in the density of the deep ocean that influenced the depth of the thermocline, as previously predicted (*9*). This cooling has been invoked by a number of hypotheses addressing the MPT (*7*, *18*). The thermal stability of the WEP, where SSTs are expected to respond thermodynamically to atmospheric radiative forcing, and the coinciding high-latitude climate stability from 900 to 1350 ky B.P. reflected by benthic $\delta^{18}O$ records, do not support changes in radiative forcing as the cause of the inferred eastern equatorial Pacific (EEP) secular cooling trend (*7*). Benthic foraminiferal carbon isotopic records, interpreted as a proxy of the thermohaline circulation, show a decrease in the $\delta^{13}C$ contrast between the North Atlantic and Pacific from 1.3 My B.P. to ~800 ky B.P. (*19*). The cooling in the EEP might reflect shallowing of the thermocline resulting from an increase in stratification produced by the deep-ocean circulation rearrangements suggested by $\delta^{13}C$ records. Model calculations suggest that a modest change in the temperature difference across the thermocline of only a few tenths of a degree can produce changes in the EEP SSTs of over 1°C (*9*).

The spectral properties of the Hole 806B SST record provide a powerful test of current hypotheses addressing Pleistocene tropical and high-latitude climate variability and the mid-Pleistocene transition. The spectral resemblance between the WEP (Hole 806B) and EEP (Hole 846) (*6*) SST records is striking (Fig. 3). Sea surface temperature variations in both end members of the equatorial Pacific are statistically coherent and in phase within the 2-ky resolution of the sites, and both records switch from 41-ky to 100-ky–dominant periods during the MPT (fig. S3). Furthermore, the early Pleistocene G-I SST range from both Hole 806B and Hole 846 is similar, 3°C and 4°C, respectively. Today, SSTs in the EEP are strongly influenced by wind-driven thermocline depth changes (*20*). In the WEP, where the thermocline is very deep (>100 m), SSTs are much less likely to be affected by thermocline depth changes (*9*, *20*). Because of this difference, interannual SST anomalies in the EEP cold tongue associated with the ENSO phenomenon are not correlated with anomalies near site 806B (Fig. 1). Further support for differences in the thermal evolution of the two equatorial Pacific end members lies in the observed long-term thermal stability of the WEP during the interval in which the EEP became progressively colder, intensifying Pacific zonal gradients after 1350 ky B.P. (Fig. 3). These observations suggest that a mechanism that invokes changes in thermocline depth (*6*) is unlikely to explain the observed warm-pool SST variability, because such a mechanism would not produce strong 41-ky cycles in SST in the WEP. On the other hand, as pointed out by Liu and Herbert (*6*), the sense of annual insolation changes in the tropics as driven by obliquity variations is in the opposite direction of that required to drive the observed tropical SST changes. We suggest instead that both end members of the equatorial Pacific responded to a common factor: atmospheric CO_2 forcing.

Consideration of the radiative forcing by different components potentially implicated in the Last Glacial Maximum suggests that atmospheric CO_2 changes are the dominant source of radiative forcing in the tropical ocean regions (*10*). A crucial role of atmospheric CO_2 in forcing tropical and Southern Hemisphere climate variability is strongly suggested by the observation that Antarctic air temperatures (*21*, *22*), tropical SSTs (*11*), and bottom-water temperatures (*23*) are in phase with atmospheric CO_2 and lead benthic foraminiferal $\delta^{18}O$ by several thousand years during the late Pleistocene. In the same manner, spectral comparisons between tropical SST records from the three sites in the tropical Pacific and foraminiferal $\delta^{18}O$ over the early Pleistocene reveal that all three SST records lead foraminiferal $\delta^{18}O$ by 3 to 7 ky at the dominant 41-ky period (table S3). The inferred lead of SST over continental ice volume rules out the hypothesis that tropical SST variability is controlled by the direct radiative influence of Northern Hemisphere continental ice sheets. The observed pattern of early and mid-Pleistocene tropical climate variability, marked by synchronous and similar magnitude SST cycles in both the warm and cold end members of the tropical Pacific, and with a clear lead of both over continental ice volume changes, is remarkably similar to late Pleistocene climate observations (*11*). The character of Pleistocene climate evolution suggests that the shift in tropical climate variability from a 41-ky to a 100-ky–dominated system (Figs. 3 and 4) is the result of changes in greenhouse forcing as mediated by the radiative effect caused by variability in atmospheric CO_2. We speculate that the global carbon system, acting as an internal self-sustained oscillator sensu (*4*), was paced by obliquity changes during the early Pleistocene (*24*); this response shifted to the eccentricity envelope of precession after the mid-Pleistocene transition. Future reconstructions of atmospheric CO_2 extending back to the MPT, projected as part of the European Project for Ice Coring in Antarctica (EPICA) (*22*, *25*), would be a direct test of this hypothesis.

References and Notes

1. N. G. Pisias, T. C. Moore Jr., *Earth Planet. Sci. Lett.* **52**, 450 (1981).
2. P. U. Clark, D. Pollard, *Paleoceanography* **13**, 1 (1998).
3. A. Berger, X. S. Li, M. F. Loutre, *Quat. Sci. Rev.* **18**, 1 (1999).
4. Y. Ashkenazy, E. Tziperman, *Quat. Sci. Rev.* **23**, 1879 (2004).
5. P. Huybers, C. Wunsch, *Nature* **434**, 491 (2005).
6. Z. Liu, D. T. Herbert, *Nature* **427**, 720 (2004).
7. T. de Garidel-Thoron, Y. Rosenthal, F. Bassinot, L. Beaufort, *Nature* **433**, 294 (2005).
8. A. H. Sobel, M. I. Held, C. S. Bretherton, *J. Clim.* **15**, 2702 (2002).
9. S. G. Philander, A. V. Fedorov, *Paleoceanography* **18**, 1045 (2003).
10. A. J. Broccoli, *J. Clim.* **13**, 951 (2000).
11. D. W. Lea, *J. Clim.* **17**, 2170 (2004).
12. W. H. Berger, T. Bickert, H. Schmidt, G. Wefer, *Proc. Ocean Drill. Program Sci. Results* **130**, 381 (1993).
13. D. W. Lea, D. K. Pak, H. J. Spero, *Science* **289**, 1719 (2000).
14. Materials and methods are available as supporting material on *Science* Online.
15. N. J. Shackleton, A. Berger, W. R. Peltier, *Trans. R. Soc. Edinb. Earth Sci.* **81**, 251 (1990).
16. Comparison of the calcite $\delta^{18}O$ records from Hole 806B and MD97-2140, a site to the northwest of Hole 806B (*7*) (fig. S2), suggests that the waters above site 806B were partly influenced by hydrological (salinity) changes on orbital time scales, with interglacial intervals becoming relatively saltier at site 806B, as previously inferred for the late Pleistocene (*13*). This inference is supported by the observation of similar SST amplitudes accompanied by different $\delta^{18}O$ amplitudes in the records from these two sites. The power in the ~90-ky band displayed by the Hole 806B $\delta^{18}O$ record during the early Pleistocene likely reflects "muted" obliquity cycles as a result of hydrological influence at this site. The $\delta^{18}O$ record from core MD97-2140 indicates clearer obliquity cycles, suggesting that hydrological influences were stronger near Hole 806B (*14*).
17. To evaluate the presence of statistically significant long-term trends in benthic $\delta^{18}O$ records from 900 ky to 1346 ky B.P., we performed linear regressions and tested the null hypothesis of zero slope (95% CI) from ODP Holes 677 (*15*), 846 (*26*), and 849 (*19*). These results indicate that there is no statistically significant long-term trend in benthic foraminiferal $\delta^{18}O$ in any of the three records. The lack of long-term trends in benthic foraminiferal $\delta^{18}O$ records at this time interval has been previously detected using independent statistical tools (*27*).
18. E. McClymont, A. Rosell-Melle, *Geology* **33**, 389 (2005).
19. A. C. Mix *et al.*, *Proc. Ocean Drill. Program Sci. Results* **138**, 371 (1995).
20. M. A. Cane, *Earth Planet. Sci. Lett.* **230**, 227 (2005).
21. J. R. Petit *et al.*, *Nature* **399**, 429 (1999).
22. EPICA Community Members, *Nature* **429**, 623 (2004).
23. N. J. Shackleton, *Science* **289**, 1897 (2000).
24. B. Saltzman, *Dynamical Paleoclimatology* (Academic Press, San Diego, CA, 2002).
25. CO_2 data from EPICA is not yet published, but the late Pleistocene record from Vostok (*22*) indicates a strong correspondence between ice D/H and CO_2. Using the EPICA δD record as a proxy for CO_2, we observe a correlation of $r = 0.70$, with zero phase between EPICA δD and the Hole 806B SST. All the major frequencies are coherent (95% CI) (*14*).
26. A. C. Mix, J. Le, N. J. Shackleton, *Proc. Ocean. Drill. Prog. Sci. Results* **138**, 839 (1995).
27. M. Mudelsee, M. Schulz, *Earth Planet. Sci. Lett.* **151**, 117 (1997).
28. Kaplan SST data provided by the NOAA-CIRES Climate Diagnostics Center, Boulder, Colorado, USA, from their Web site at www.cdc.noaa.gov.
29. B. E. Bemis, H. J. Spero, J. Bijma, D. W. Lea, *Paleoceanography* **13**, 150 (1998).

30. Supported by NSF (OCE0317611) and CONACYT-UCMEXUS. Laboratory assistance from D. Pak and J. Horton and mass spectrometer operation by G. Paradis was crucial to the success of this study. We thank H. Spero for isotopic analyses at University of California Davis; T. Kostadinov and P. Huybers for their support in signal processing; J. Kennett and M. Sarnthein and two anonymous reviewers for their comments and suggestions; and Z. Liu for discussion. Evolutionary spectral analysis was computed using software provided by P. Huybers.

Supporting Online Material

www.sciencemag.org/cgi/content/full/1115933/DC1
Materials and Methods
SOM Text
Figs. S1 to S5
Tables S1 to S3
References

9 June 2005; accepted 5 October 2005
Published online 13 October 2005;
10.1126/science.1115933
Include this information when citing this paper.